Engineering xxx (xxxx) xxx

Contents lists available at ScienceDirect

Engineering

journal homepage: www.elsevier.com/locate/eng

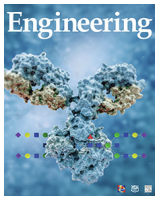

Research
Unmanned Intelligent Cluster—Article

Robot Pilot: A New Autonomous System Toward Flying Manned Aerial Vehicles

Zibo Jin, Daochun Li *, Jinwu Xiang

School of Aeronautic Science and Engineering, Beihang University, Beijing 100191, China

ARTICLE INFO

Article history:
Received 24 November 2021
Revised 15 August 2022
Accepted 27 October 2022
Available online 3 April 2023

Keywords:
Helicopter
Robot pilot
Flight control
Unmanned system

ABSTRACT

The robot pilot is a new concept of a robot system that pilots a manned aircraft, thereby forming a new type of unmanned aircraft system (UAS) that makes full use of the platform maturity, load capacity, and airworthiness of existing manned aircraft while greatly expanding the operation and application fields of UASs. In this research, the implementation and advantages of the robot pilot concept are discussed in detail, and a helicopter robot pilot is proposed to fly manned helicopters. The robot manipulators are designed according to the handling characteristics of the helicopter-controlling mechanism. Based on a kinematic analysis of the robot manipulators, a direct-driving method is established for the robot flight controller to reduce the time delay and control error of the robot servo process. A supporting ground station is built to realize different flight modes and the functional integration of the robot pilot. Finally, a prototype of the helicopter robot pilot is processed and installed in a helicopter to carry out flight tests. The test results show that the robot pilot can independently fly the helicopter to realize forward flight, backward flight, side flight, and turning flight, which verifies the effectiveness of the helicopter robot pilot.

1. Introduction

The fundamental reason for developing any unmanned aircraft system (UAS) is to remove the pilot from the aircraft in order to realize operational benefits and reduce pilots' risks [1]. With the development impetus for the innovative technologies of flight perception [2], control methods [3], and complete autonomy [4–7], UASs have received substantial interest from the research community and general public alike in recent years [8]—especially small unmanned aerial vehicles (UAVs) and multi-rotors, whose low cost, convenient use, and good maneuverability provide favorable advantages in their application in various fields. However, small or medium-sized UAVs are insufficient to meet the demands of high payloads and long flight distances for the wider range of flight missions currently realized by manned aircraft. However, considerable cost and a long research period are required to develop a large-scale UAS with a mature platform and large load capacity, posing a challenge for the further development and application of UASs.

One way to quickly generate such a large-scale UAS is to perform unmanned modifications on existing manned aircraft [9]. This method eliminates the need to design a UAS from scratch and has already been applied to specific aerial vehicles such as the QF-16 (modified from the F16) [10], the Dominator (modified from the DA42) [11], and the unmanned Little Bird helicopters [12–14]. In general, the conversion process from a manned aircraft to a UAS requires the installation of servomotors on the flying surfaces to actuate the control surfaces of the aircraft, or a reconstruction of the control loop of the existing flight control system. The high cost and complexity of such processes have become the main limiting factors in unmanned modifications. The conversion process is irreversible and must be repeated all over again when modifying another vehicle [15]. Furthermore, excessive modifications may hamper the flight performance or airworthiness of the original aircraft.

In comparison with modifying a manned aircraft, the idea of using robots to assist or replace human pilots to fly manned aircraft has been raised and considered as a potential research field in recent years. Research and development institutions have given considerable attention to robot pilot systems and have launched explorations on them. The main advantage of the robot pilot concept is that it is a noninvasive way to convert manned aircraft into

* Corresponding author.
E-mail address: lidc@buaa.edu.cn (D. Li).

https://doi.org/10.1016/j.eng.2022.10.018

Please cite this article as: Z. Jin, D. Li and J. Xiang, Robot Pilot: A New Autonomous System Toward Flying Manned Aerial Vehicles, Engineering, https://doi.org/10.1016/j.eng.2022.10.018

UAS, making the conversion process reversible. The new UAS retains the load capacity and safety assurances of the original manned aircraft for carrying out long flights or transportation missions. Moreover, the robot pilot can serve as a co-pilot to increase the automation level of an existing aircraft and help human pilots to improve their flight performance, thus providing a brand-new perspective on newly developing assisted-piloting technologies such as pilot assistants [16,17], optional piloted vehicles [18], intelligent cockpits [19–21], and single-pilot operations (SPO) [22,23]. In addition, the robot pilot will not hamper the airworthiness or flight performance of the original aircraft, which is conducive to solving the current hot topic of the integration of UASs and manned aircraft within the same airspace [1]. From a scientific research perspective, a robot pilot can carry multiple sensors and integrate diverse manipulators, providing a powerful platform for emerging research interests in the field of aerospace, including high-level autonomy [24], flight control technologies, human–robot collaboration, and hybrid-augmented intelligence [25].

Related projects have focused on developing robot pilots or automated co-pilot systems in recent years. The Defense Advanced Research Projects Agency (DARPA) announced the DARPA Robotics Challenge (DRC), which aims to develop robots capable of executing complex tasks in dangerous, degraded, and human-engineered environments. The Aircrew Labor In-cockpit Automation System (ALIAS) Co-Pilot robot was introduced to support the autopilot system in the crew cabin and to improve the connections between human pilots and increasingly powerful computers and sensors [26–28]. The ALIAS Co-Pilot robot has undergone flight tests in multiple aircraft under the supervision of human pilots. In 2022, the ALIAS program carried out flight tests on UH-60 helicopters [29]. The Korea Advanced Institute of Science and Technology (KAIST) verified that a humanoid robot could operate an aircraft by designing a robot pilot called PIBOT in 2016 [15,30,31]; the name combines the words "pilot" and "robot." The first-generation PIBOT was a scaled-down version, while the second generation adopted a proportionate humanoid joint mechanism. A cascade proportional–integral–differential (PID) control method was used to allow PIBOT to fly the aircraft in a flight simulator. The US Air Force Research Laboratory Center for Rapid Innovation (CRI) presented ROBOpilot as a modular system that aims to rapidly convert existing manned aircraft into autonomous unmanned aircraft [32]. ROBOpilot was processed and completed its second flight tests on a Cessna 206 in 2020 [33]. In our previous research, we proposed a humanoid robot pilot and conducted flight tests on a flight simulator [34].

The above projects and research have verified the feasibility of a robot pilot to varying degrees through flight simulators and real aircraft experiments. Nevertheless, detailed investigations of the servo design, control method, system integration, and flight performance of the robot pilot are still lacking. More specifically, the robot servo design must achieve control accuracy and sensitivity while minimizing its occupied space in order to reduce interference with the control of other facilities in the cockpit. The robot servo time delay will significantly affect the overall flight performance, so it is necessary to establish appropriate flight controllers and robot control methods. The functional integration of the robot pilot requires the specific definition of robot control methods or the realization of assisted piloting under different flight modes, yet these essential issues have rarely been studied in previous research. Moreover, the existing research mainly describes the use of a robot pilot for fixed-wing aircraft, while little research exists on the use of a robot to independently pilot a helicopter. Since the operating requirements and controlling complexity of helicopters are higher than those of fixed-wing aircraft, this endeavor presents challenges in terms of the manipulation and flight control design of the robot pilot.

In this research, we first present a detailed investigation of the helicopter robot pilot. The reasons for and advantages of using a robot pilot to fly an aircraft are discussed. Robot manipulators are designed according to the helicopter-controlling mechanisms, and a robot flight controller is determined using a direct-driving method based on a kinematic analysis of the robot manipulators. A flight simulator is established to conduct flight simulations and is further integrated into a ground station system to assist in the robot piloting. Finally, a prototype of the helicopter robot pilot is processed and installed in a real helicopter to carry out flight tests. The test results verify the effectiveness of the robot pilot presented in this research.

The remainder of the paper is organized as follows: We briefly describe the conception and functional requirements of the robot pilot and establish the helicopter cockpit model in Section 2. In Section 3, we describe the design of the robot manipulators of different helicopter-controlling mechanisms. In Section 4, we detail the overall control framework of the robot pilot and examine the control methods through flight simulations. In Section 5, we describe building the ground station and prototype of the robot pilot and carrying out flight tests. Finally, we summarize our conclusions in Section 6.

2. Robot system integration

The robot pilot is a newly developed unmanned system that requires multiple functional subsystems to realize reliable autonomous flight. In this section, we attempt to provide a general description of the robot pilot and different flight modes. On this basis, we propose an overall design scheme for a specific robot pilot that can independently fly a manned helicopter. The robot pilot essentially belongs to the domain of a robot system or unmanned system. It integrates an independent sensor system and a control system to interact with the cockpit electronics and machinery like a human pilot, allowing the robot pilot to be combined with a manned aircraft to form a new UAS, as shown in Fig. 1. In this manner, a manned aircraft can be converted into an automated mode in a very short time without modification, which greatly improves the flexibility and mission ranges of manned aircraft. In general, the flight operations of the robot pilot can be divided into a fully autonomous flight mode and a limited autonomous/assisted-piloting mode. For the fully autonomous flight mode, the robot pilot can independently fly a manned aircraft to accomplish flight missions in high-risk environments such as nuclear radiation areas, which can be harmful or dangerous to human pilots. For the assisted-piloting mode, the robot system can cooperate with a human pilot to decrease the number of required crew members and reduce the human pilot's tiredness. Both flight modes require a mature ground station system to support the robot's piloting. The ground station provides complete communication links to realize the monitoring of the robot operations, flight state perception, and remote-control functions, which are essential for reliable flight and safety assurances.

Based on the factors described above, we propose a helicopter robot pilot with the overall design scheme illustrated in Fig. 2. The robot pilot, helicopter, and ground station combine to form an entire unmanned helicopter system. The robot pilot consists of robot manipulators, a robot flight controller, a supporting structure, and a visual perception system. The helicopter robot pilot uses the manipulators to connect to and control the helicopter-controlling mechanisms in order to fly the helicopter. The robot flight controller is embedded into the robot pilot in order to estimate the flight state and send out control signals to the robot manipulators. The supporting structure assembles the robot manipulators and other equipment. The visual system of the robot

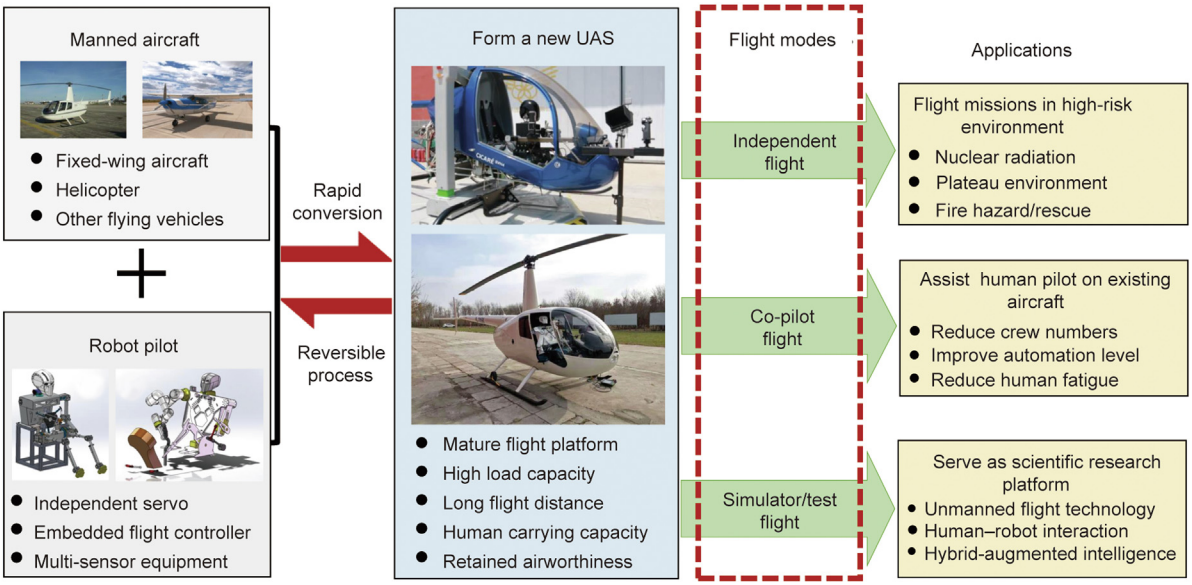

Fig. 1. Advantages and flight modes of the robot pilot.

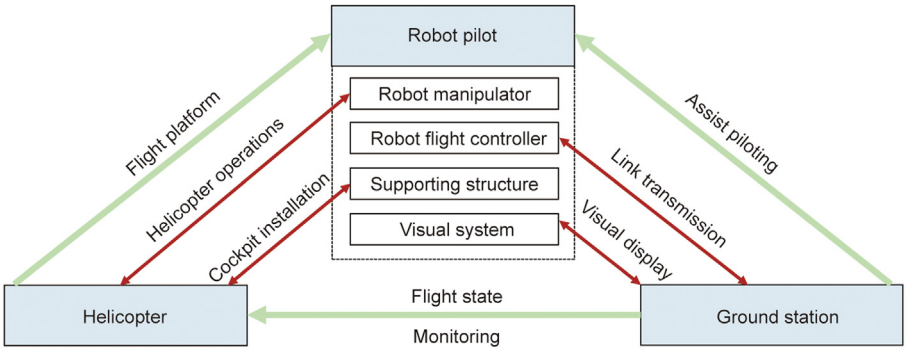

Fig. 2. The system integration of the robot pilot.

pilot is used to capture and record the real-time scene outside the cockpit during the flight.

A light helicopter called SVH-4 was selected as the flight platform of the robot pilot in this research. The SVH-4 helicopter has a total length of 7.28 m and a total height of 2.48 m. It uses a Rotax912ULS diesel engine with a take-off weight of 460 kg and a payload of 180 kg. Unlike typical manned helicopters, the SVH-4 helicopter has a supporting platform to limit the helicopter's flight height and prevent the helicopter from rollover, crashing, and other accidents during the flight. The connection between the supporting platform and the helicopter is realized by a cross bar that penetrates under the helicopter rotor. The cross bar provides two degrees of freedom (2-DOF) for the helicopter pitch and roll motions. The struts of the cross bar provide the vertical and yaw motions of the helicopter. The damping of the cross bar and the struts is very small, so the helicopter retains its flight performance and has complete aerodynamics similar to those of a Robinson-22 helicopter. The moving platform slides along the ground through the bottom pulley, which inevitably introduces discontinuous ground friction when the helicopter moves horizontally. Apart from this disadvantage, the SVH-4 was considered to be suitable for carrying out flight tests with the helicopter robot pilot and verifying the robot performance with very little risk.

The helicopter robot pilot is designed to be mounted in the helicopter cockpit and to operate on the helicopter-controlling mechanisms. It is necessary to accurately measure the internal geometries and lever positions of the cockpit, which serve as the design basis for the robot manipulators. A cockpit model of the SVH-4 was established through these measurements, as shown in Fig. 3. The main control mechanisms of the SVH-4 helicopter are the control stick, collective, and pedals. The control stick is located in the center front of the pilot seat, while the collective is located on the left side of the pilot seat and rotates around the bearing axis. The pedals are on both sides of the instrument panel. The motion

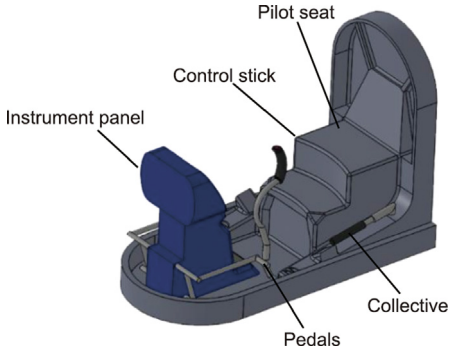

Fig. 3. Helicopter cockpit.

space of the helicopter-controlling mechanisms was established to obtain the limit position and motion constraint. The motion space of the control stick is over a curved surface, as shown in Fig. 4, and the motion space of the collective and pedals are along planes.

3. Robot manipulators and kinematic analysis

The robot manipulator design directly determines the controlling performance of the robot pilot. However, such a design has rarely been mentioned or studied in previous research. We adopted a modular design for the robot manipulators, which were separately designed according to the handling characteristics of the corresponding controlling mechanisms. All the robot manipulators can be assembled and integrated in a flexible way, which increases the robot's ability to adapt to the cockpits of different helicopters. In order to command the robot manipulators into the desired poses, a kinematic analysis was carried out to obtain the geometric mappings between the joint angles and end positions of the robot manipulators.

3.1. Manipulator of the control stick

The helicopter control stick rotates around the stick bottom and controls the swashplate in the longitudinal and lateral directions, resulting in a corresponding rotor thrust, which in turn changes the pitch and roll motions of the helicopter. The manipulator of the control stick must have high maneuverability and high accuracy, since the control stick is operated frequently at all times during a flight. The helicopter control stick is the most distinctive control mechanism and is significantly different from that of a fixed-wing aircraft. For the robot manipulator of the control stick, the main issue is to balance the control accuracy, mechanism volume, and servo sensitivity. In our previous studies, we designed various manipulators for a helicopter control stick [34], as shown in Fig. 5. The delta robot shows good manipulation accuracy, but the response speed does not adequately meet the flight control requirements. The multi-freedom mechanical arm decouples the horizontal and vertical directions through multiple motors, but the control accuracy is particularly vulnerable to installation errors. In our research on the cooperative robot pilot, we designed a planar servo mechanism involving a synchronous belt, which has a compact structure and high response speed. However, it requires a suitable installation environment in the helicopter cockpit and is sensitive to fuselage vibrations during the flight. In this research, we designed a six degrees of freedom (6-DOF) manipulator to operate the control stick for the helicopter robot pilot. This 6-DOF manipulator has both good control accuracy and high response speed [35]. The manipulator base can be firmly installed on the inner/outer floor or support of the helicopter cockpit, and the initial position can be flexibly adjusted to avoid interference with other control mechanisms.

The 6-DOF manipulator of the robot pilot is shown in Fig. 6. It consists of a base and six linkages, which are connected by six rotational joints. The manipulator base was designed to be installed on the helicopter landing gear outside the cockpit on the right side. The end-effector is driven by the joints and has 6-DOF. A universal joint is connected to the end-effector to grasp the helicopter control stick. The universal joint is used to eliminate the DOF in the *Z* direction, since the end-effector moves over a curved surface.

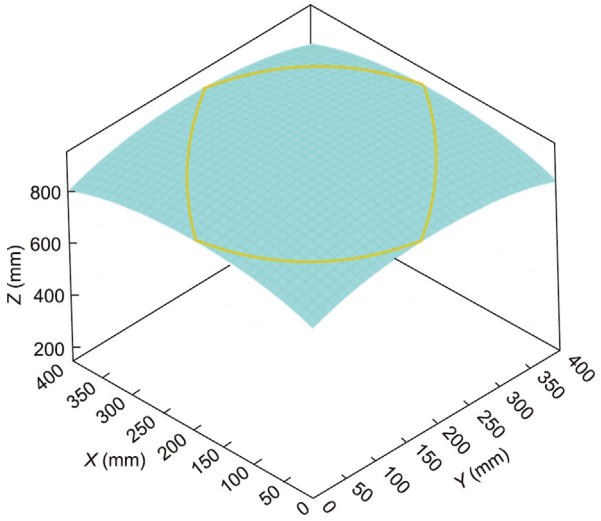

Fig. 4. Motion space of the control stick.

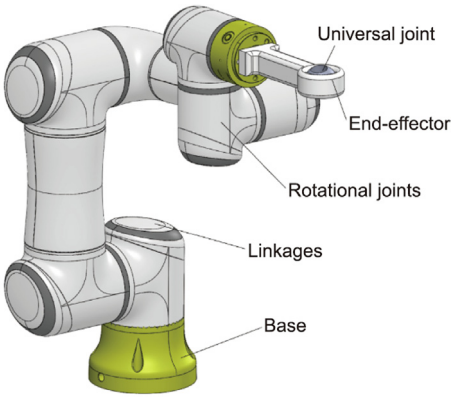

Fig. 6. The 6-DOF manipulator.

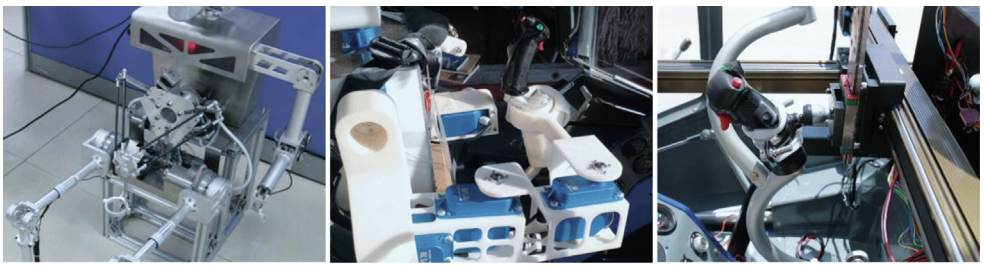

Fig. 5. Different robot manipulators for the helicopter control stick. (a) The delta robot; (b) a multi-freedom mechanical arm; (c) an *XY* servo mechanism involving a synchronous belt.

This is a very effective way to prevent the robot manipulators from getting stuck during their movement.

The aim of the kinematic analysis of the 6-DOF manipulator was to determine the rotation angles of the manipulator joints, when given the required position of the end-effector. First, a coordinate system arrangement was established from the base to the end-effector, as shown in Fig. 7. The Denavit–Hartenberg (D–H) parameters were used to describe the theoretical structure of the 6-DOF manipulator. Once the D–H coordinate system had been established for each link, a homogeneous transformation matrix $\boldsymbol{Ai}$, as given in Eq. (1), could be easily developed that relates the ith coordinate frame to the $(i-1)$th coordinate frame,

$$\boldsymbol{A}_i = \begin{bmatrix} \cos\theta_i & -\sin\theta_i\cos\alpha_i & \sin\theta_i\sin\alpha_i & a_i\cos\theta_i \\ \sin\theta_i & \cos\theta_i\cos\alpha_i & -\cos\theta_i\sin\alpha_i & a_i\sin\theta_i \\ 0 & \sin\alpha_i & \cos\alpha_i & d_i \\ 0 & 0 & 0 & 1 \end{bmatrix} \tag{1}$$

where θ_i and α_i are the joint angle and the link torsion angle, and d_i are the joint offset.

The matrix $\boldsymbol{T}$ is used to represent the pose of the end-effector, which is composed of an orientation matrix $\boldsymbol{R}$ and a position vector $\boldsymbol{P}$, as shown in Eq. (2). The orientation matrix represents the orientation of the manipulator end-effector, and the position vector points from the origin of the base coordinate system to the origin of the sixth coordinate system.

$$\boldsymbol{T} = \begin{bmatrix} \boldsymbol{R} & \boldsymbol{P} \\ 0 & 1 \end{bmatrix} \tag{2}$$

$\boldsymbol{T}$ is calculated using the chain product of the successive coordinate transformation matrices of $\boldsymbol{A}_i$, as shown in Eq. (3). When using the 6-DOF manipulator to control the control stick, the pose matrix $\boldsymbol{T}$—that is, the desired position of the end-effector—is obtained first. The corresponding joint angles θ_1, θ_2, θ_3, θ_4, θ_5, and θ_6 are then obtained by the inverse kinematics equations.

$$\boldsymbol{T} = \boldsymbol{A}_1\boldsymbol{A}_2\boldsymbol{A}_3\boldsymbol{A}_4\boldsymbol{A}_5\boldsymbol{A}_6 \tag{3}$$

In this research, an analytical method was used to obtain the inverse solutions of the joint angles; the detailed kinematic equations can be found in Refs. [36–38]. As the manipulator has 6-DOF and flexibility within the space, there are multiple inverse solutions for one pose matrix $\boldsymbol{T}$. The shortest travel law is considered to be the criterion to obtain the best solution [36], as given in Eq. (4). The inverse solution that has the minimum Δ is selected, and the joint angles are obtained.

$$\Delta = \sum_{i=1}^{6} |\theta_{ic} - \theta_{il}| \tag{4}$$

θ_{ic} and θ_{il} represent the current angle and the last angle of the ith joint, respectively.

3.2. Manipulator of the pedals

The pedals change the thrust of the tail rotor to control the helicopter's yaw motion. When flying a helicopter, the operation of the pedals does not require particularly fast movement. Here, the manipulator of the pedals takes the form of a mechanical leg to achieve human-like operations. As shown in Fig. 8, the mechanical leg consists of the base, the hip joint, the thigh, the knee joint, and the calf. The base is fixed on the pilot seat, and the calf end is connected to the pedal. The hip joint driven by the servo motor is the main executive, while the knee joint is a passive joint. The pedals of the SVH-4 helicopter move in tandem—that is, when one pedal moves down, the other pedal will move up simultaneously. Therefore, the mechanical leg can be used to pull and raise one pedal in order to achieve the same effect of a human pilot controlling both pedals.

The kinematic relations between the hip joint angle and the pedal rotational angle are obtained as follows. As shown in Fig. 9, the mechanical leg and the pedal combine to form a closed-loop four-bar mechanism. The hip joint, knee joint, and sole are simplified to points H, K, and S, respectively. The length of the thigh, the length of the calf, and the equivalent rotation radius of the pedal are presented as l_t, l_c, and l_p, respectively. When the robot pilot is installed in the cockpit, the relevant positions of the hip joint and the pedal rotation center are fixed and measurable. By establishing the coordinate system at the pedal rotation center O_p, the coordinates of the hip joint are assumed to be (H_x, H_y). The kinematic relations between the hip joint angle and pedal rotational angle can then be obtained as shown in Eq. (5). Therefore, when given the required pedal rotational angle φ_1, the robot pilot can directly determine the corresponding hip joint angle φ_2. The change curve between the hip joint angle and the pedal rotational angle is illustrated in Fig. 10. By designing appropriate length parameters of the thigh and calf, the rotational angle ratio can be made to be quasi-linear within the operating limit of the pedal. This method can be used for the direct-driving method of the subsequent flight control system design.

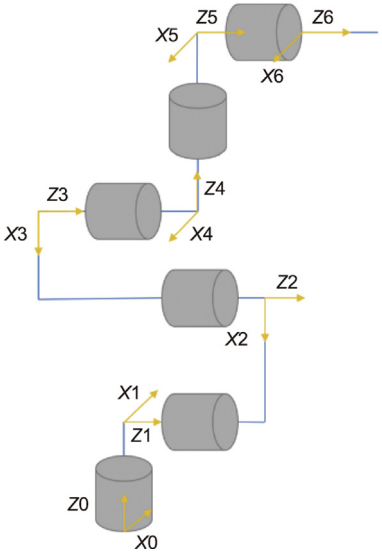

Fig. 7. The coordinate system of the 6-DOF manipulator. Xi and Zi (i = 0, 1, 2, . . ., 6) are the coordinate axis in the local coordinate system of each joint.

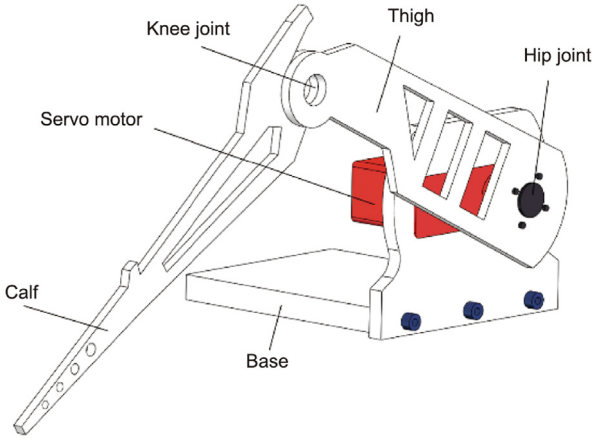

Fig. 8. The mechanical leg.

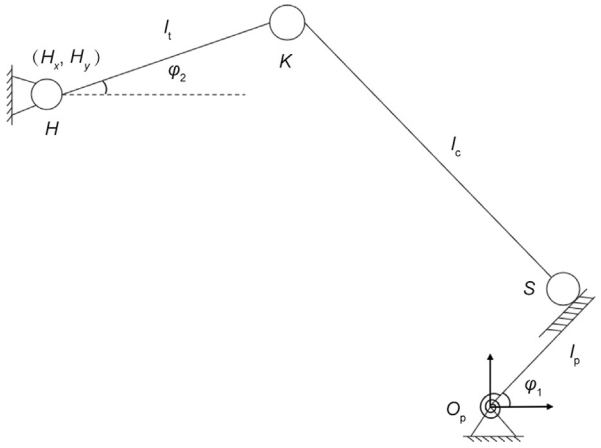

Fig. 9. Schematic diagram of the mechanical leg. *H*, *K*, and *S*: the points of hip joint, knee joint, and sole, respectively; O_p: the pedal rotation center; (H_x, H_y): the coordinates of the hip joint; φ_1: the pedal rotational angle; φ_2: the hip joint angle; l_t, l_c, and l_p: the length of the thigh, the length of the calf, and the equivalent rotation radius of the pedal, respectively.

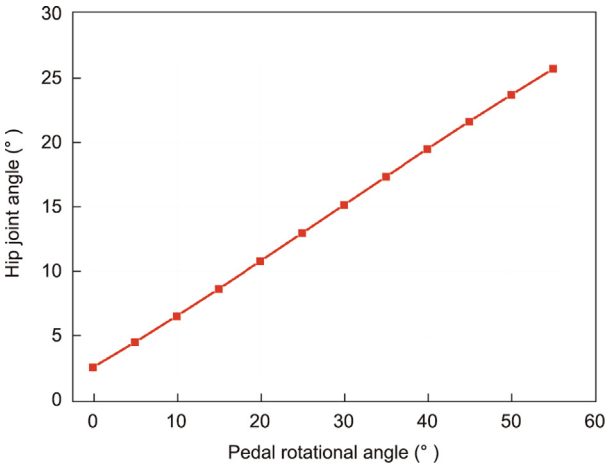

Fig. 10. The change curve of the hip joint angle and pedal rotational angle.

$$\begin{cases} x_1^2 + x_2^2 + l_t^2 - l_c^2 + 2l_t x_1 \cos\varphi_2 + 2l_t x_2 \sin\varphi_2 = 0 \\ x_1 = H_x - l_p \cos\varphi_1 \\ x_2 = H_y - l_p \sin\varphi_1 \end{cases} \tag{5}$$

where x_1 and x_2 are the intermediate variables.

3.3. Manipulator of the collective

When raising the collective, the attack angle of the rotor blade is increased, causing the lifting movement of the helicopter. The manipulator of the collective is designed as a mechanical arm to complete the lifting and dropping action. The mechanical arm consists of the arm support, the servo motor, the swing arm, the elbow joint, and the connecting rod, as shown in Fig. 11. The arm support is fixed on the left side of the robot pilot. The upper end of the connecting rod links to the swing arm, while the lower end connects to the collective. The swing arm has multiple mounting holes, so the mounting position of the connecting rod can be adjusted.

The kinematic relations between the elbow joint angle and the collective rotational angle are obtained as follows. The mechanical arm and the collective can be considered as a closed-loop four-bar mechanism, as shown in Fig. 12. The elbow joint and collective rotation center are simplified as *E* and O_c, respectively. *U* and *L* represent the two ends of the connecting rod. The coordinate system

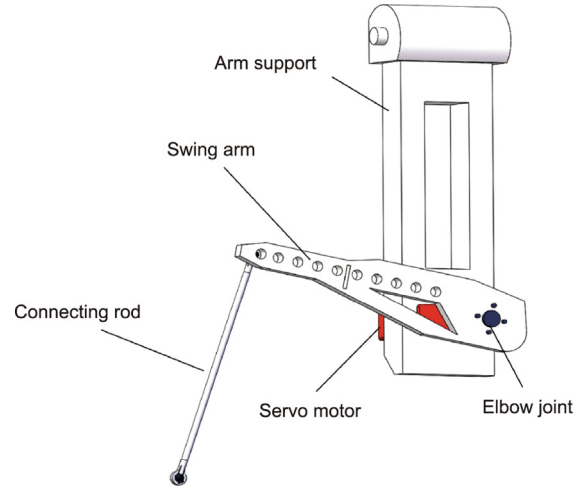

Fig. 11. Mechanical arm.

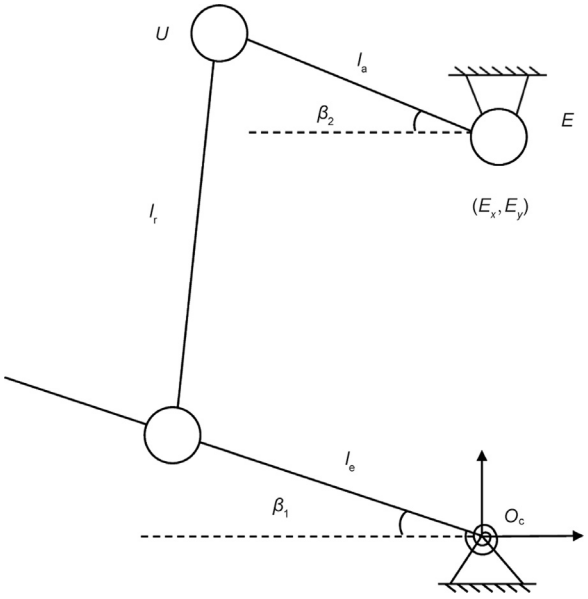

Fig. 12. Schematic diagram of the mechanical arm. *E* and O_c: the elbow joint and collective rotation center, respectively; *U* and *L*: the two ends of the connecting rod; (E_x, E_y): the coordinate of the arm support; l_a and l_r: the length of the swing arm and the connecting rod, respectively; l_e: the equivalent rotation radius of the collective; β_1 and β_2: the collective rotational angle and elbow joint angle, respectively.

is set up with *O* as the origin. The coordinate of the arm support is certain and is assumed to be (E_x, E_y). Let the length of the swing arm and the connecting rod be l_a and l_r, respectively. l_e is the equivalent rotation radius of the collective. The collective rotational angle and elbow joint angle are illustrated as β_1 and β_2, respectively. The kinematic relation between β_1 and β_2 is shown in Eq. (6), and the change curve is illustrated in Fig. 13. Here, the linear relationship of the rotational angle ratio is not ideal compared with that of the mechanical leg. However, considering that the sensitivity and accuracy requirements of the collective control are relatively loose, this linearization error is acceptable within the collective control range.

$$\begin{cases} x_3^2 + x_4^2 + l_a^2 - l_r^2 - 2l_a x_3 \cos\beta_2 + 2l_a x_4 \sin\beta_2 = 0 \\ x_3 = E_x - l_e \cos\beta_1 \\ x_4 = E_y - l_e \sin\beta_1 \end{cases} \tag{6}$$

where x_3 and x_4 are the intermediate variable.

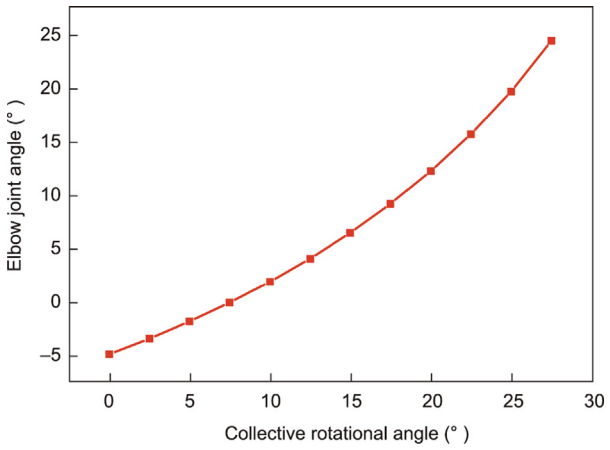

Fig. 13. The change curve of the elbow joint angle and collective rotational angle.

4. Control system of the robot pilot

4.1. Control scheme of the robot–helicopter system

The control flow of the robot pilot can be divided into the outer loop of the helicopter flight control and the inner loop of the robot servo control. As shown in Fig. 14, the helicopter control loop calculates the control signals according to the helicopter flight state and commands, while the robot control loop receives the control signals and drives the manipulators to control the helicopter-controlling mechanisms. In the common control flow, the robot pilot first needs to calculate the desired lever position of each helicopter-controlling mechanism and the desired position of the manipulator end-effectors of the robot pilot according to the pulse width modulation (PWM) signal output by the helicopter flight controller. Next, the manipulator joint angles are obtained based on the kinematic relations discussed in Section 3. Finally, the robot pilot drives the manipulator joints to cause the manipulator end-effector to reach

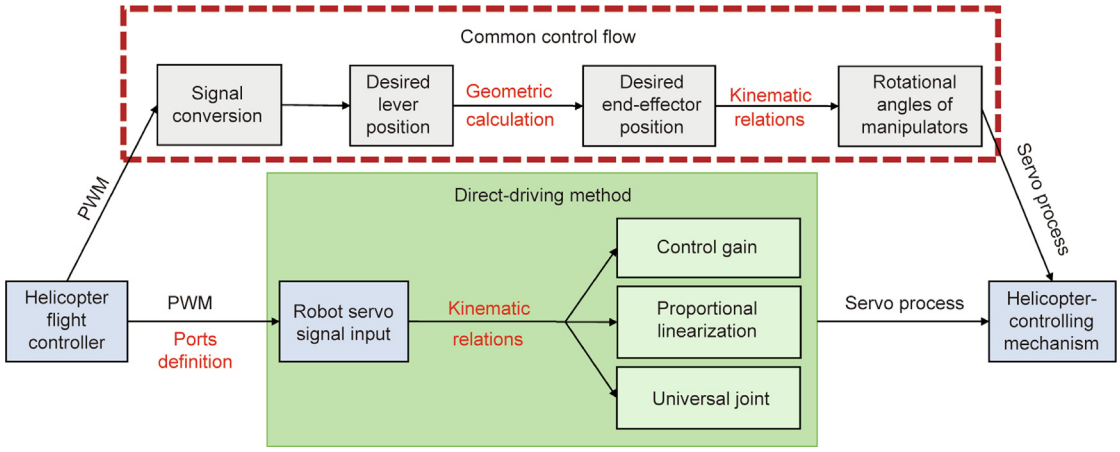

Fig. 14. Control flow of the robot–helicopter system. PWM: pulse width modulation.

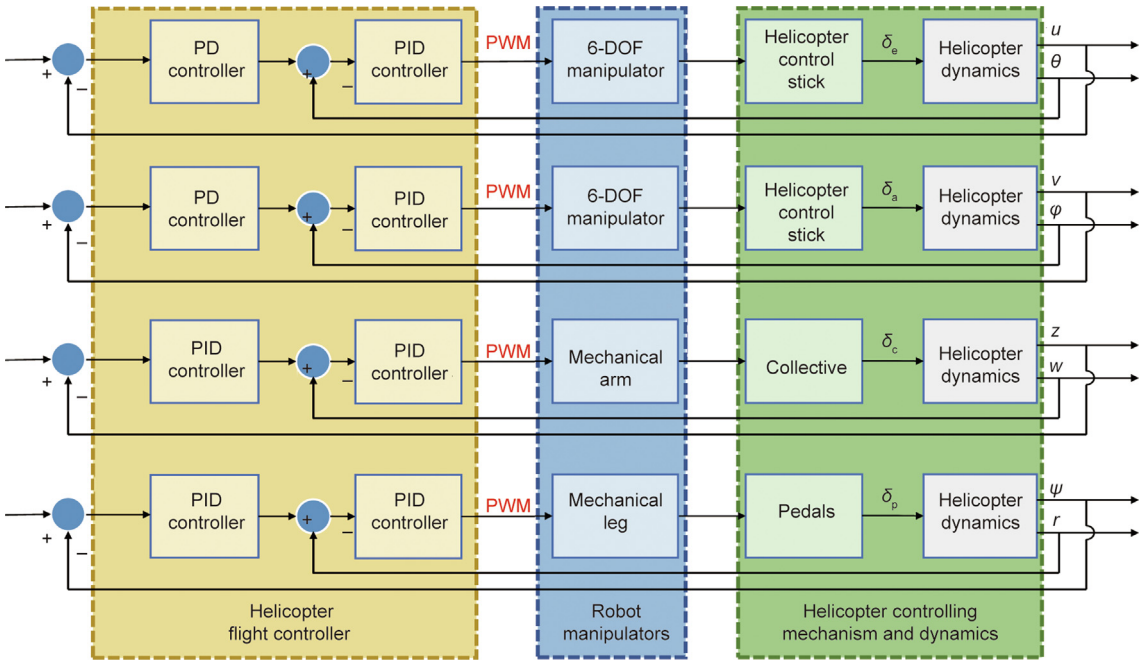

Fig. 15. Overall control scheme of the robot–helicopter system. PD: proportional–differential; u, v, and w: the helicopter's linear velocities; θ, φ, and ψ: the pitch, roll, and yaw angles of the helicopter altitude, respectively; z: the flight height of the helicopter; δ_c and δ_p: the collective control input of the main rotor blade and the tail rotor blade, respectively; δ_e and δ_a: the cyclic control inputs giving the explicit pitch in the longitude and lateral directions, respectively.

the desired position. In this way, the robot control loop contains complex calculating processes and signal conversions. The robot controller and helicopter flight controller are relatively independent, which could result in an increased time delay and controlling errors. Also, the end position of the helicopter control stick moves along a curved surface; thus, driving the manipulator end-effector to the desired position involves the problems of trajectory planning and motion constraint.

In this research, we propose a direct-driving method to directly drive the robot manipulators through the PWM signal output from the helicopter flight controller, as shown in Fig. 14. For the 6-DOF manipulator, we use a universal joint to resolve the motion constraint and design the input port to receive PWM signals. Therefore, the 6-DOF manipulator only needs to control the end-effector to move in the horizontal range according to the PWM signals of longitudinal and lateral decoupling. For the mechanical arm and mechanical leg, we use the linearization ratio based on the obtained kinematic relations as the control gain of the driving joint to let the helicopter flight controller directly drive the robot manipulators through PWM signals. The direct-driving method eliminates the signal conversion process and calculation process, thereby reducing the time delay and control error of the robot servo process to the greatest extent. Moreover, with this method, it is not necessary to modify the structure or output form of the helicopter flight controller, so the robot pilot can be adapted to various flight control algorithms and hardware.

We adopted a modular scheme for the helicopter robot pilot, with independent manipulators for each helicopter-controlling mechanism. To facilitate the realization and parameter tuning of different robot manipulators, the helicopter flight control in this research was divided into four control channels, as shown in Fig. 15. Compared with general automatic helicopter flight control, the robot–helicopter system contains the controlling delay of the robot servo and the operating error of the helicopter-controlling mechanism, which is mutable and difficult to quantify. A dynamic model of the robot–helicopter system was difficult to obtain, so a model-free PID control method was used as the flight controller of the robot pilot. Based on the kinematic analysis and the direct-driving method, the robot pilot can directly drive the helicopter control mechanism to the desired position without overshoot or error corrections. Therefore, the controlling delay of the robot servo process is limited in a small range, while the PID control method can already obtain good performance. The PID controller continuously calculates the error value and applies a correction to make the system output approach the target value. The time-domain output equation of the PID controller is shown in Eq. (7). The error value $e(t)$ is obtained according to the target value and the actual output value, where t is time variable. The controller output $u(t)$ is based on linear combinations of the error value in proportional, integral, and derivative terms (denoted as P, I, and D). The inner loop of the cascade PID controllers is built to control the helicopter altitude, and the outer loop controls the helicopter's linear velocities.

$$u(t) = K_P e(t) + K_I \int e(t)dt + K_D \frac{de(t)}{dt} \tag{7}$$

where K_P, K_I, and K_D are the PID parameters.

It should be mentioned that helicopters have multiple flight mode transitions arising from the complicated aerodynamic nature of thrust generation, while the control channels are strongly coupled. Various flight control methodologies have been developed for the flight control system of helicopters to improve flight performance, but these lie beyond the scope of this research. We used simple and decoupling PID controllers to bypass the complex dynamic modeling process of the robot–helicopter system. The control parameters of the PID controllers are easy to understand and tune, effectively reducing the risks of the flight tests.

4.2. Flight simulations of the robot–helicopter system

Flight simulations of the robot–helicopter system were conducted for initial validation before flight tests were carried out. The simulations were also helpful for preliminarily setting and tuning the PID parameters of the robot flight controller based on the approximate models. The flight simulation of the robot–helicopter system consisted of the helicopter model, robot flight controller, and approximate models used for simulating the servo process of the robot manipulators and the transfer process of the helicopter-controlling mechanism. Since a dynamic model of the SVH-4 helicopter has not been established, a dynamic model of the OH-6A helicopter—whose weight and configurations are similar to those of the SVH-4 helicopter—was used as the helicopter model in the simulation. The OH-6A helicopter model is based on the aerodynamic test data [39]: The helicopter exhibits

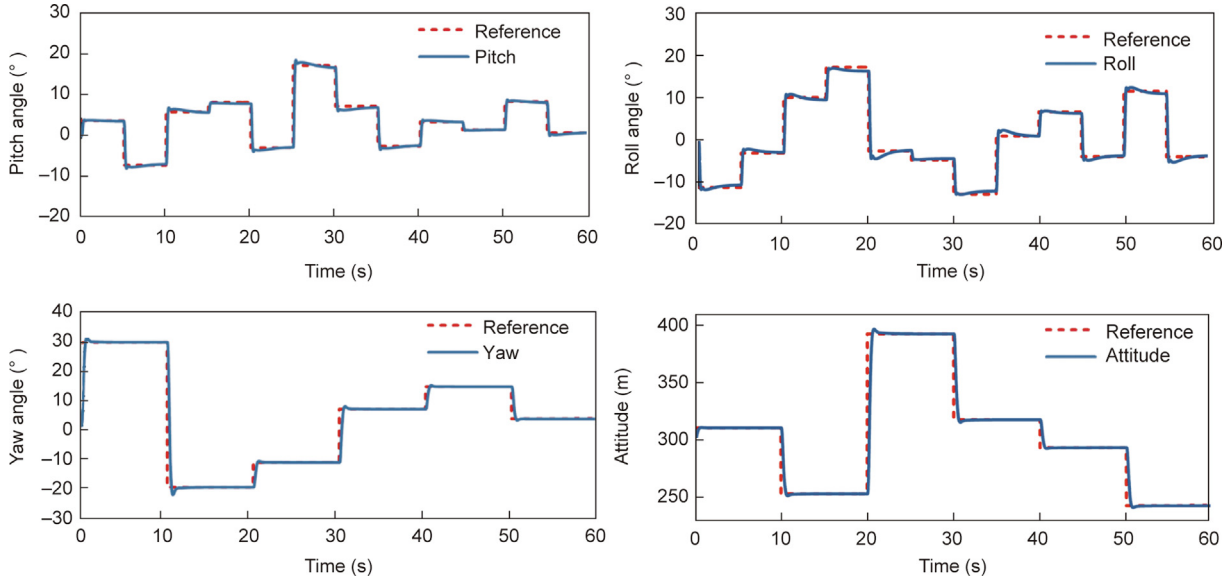

Fig. 16. Command tracking of the robot–helicopter system.

Fig. 17. Helicopter installation of the robot pilot.

6-DOF rigid-body dynamics, and the flight dynamic equations are as follows

$$\dot{\boldsymbol{V}} = \frac{\boldsymbol{F}}{m} - \boldsymbol{\Omega V} \tag{8}$$

$$\dot{\boldsymbol{S}} = \boldsymbol{I}^{-1}\boldsymbol{M} - \boldsymbol{I}^{-1}\boldsymbol{\Omega I S} \tag{9}$$

where $\boldsymbol{V}$ is the helicopter linear velocity and $\dot{\boldsymbol{V}}$ is the linear acceleration; $\boldsymbol{S}$ represents the angular velocity and $\dot{\boldsymbol{S}}$ is the angular acceleration; $\boldsymbol{I}$ is the moment of the helicopter inertial matrix; $\boldsymbol{\Omega}$ is the angular rate antisymmetric matrix; m is the mass of the helicopter; $\boldsymbol{F}$ and $\boldsymbol{M}$ are the forces and moments of the components of the helicopter, respectively.

For the helicopter dynamic model, $\boldsymbol{F}$ and $\boldsymbol{M}$ are generated by complicated aerodynamic forces, which makes it difficult to establish a fully dynamic model. We adopted a linearized dynamic model in this research to simulate the helicopter's dynamic responses. A linear-parameter-varying (LPV) helicopter dynamic model was established, as shown in Eq. (10). The kinematic equations are obtained by a conversion matrix $\boldsymbol{R}_{\mathrm{BG}}$ from the body coordinates to the ground coordinates, as shown in Eq. (11).

$$\dot{\boldsymbol{x}} = \boldsymbol{A}_s\boldsymbol{x} + \boldsymbol{B}_s\boldsymbol{u} \tag{10}$$

$$\boldsymbol{R}_{\mathrm{BG}} = \begin{bmatrix} \cos\theta\cos\psi & \sin\theta\sin\psi\cos\psi - \cos\varphi\sin\psi & \sin\theta\cos\varphi\cos\psi + \sin\varphi\sin\psi \\ \cos\theta\cos\psi & \sin\theta\sin\varphi\sin\psi + \cos\varphi\cos\psi & \sin\theta\cos\varphi\cos\psi - \sin\varphi\sin\psi \\ -\sin\theta & \sin\varphi\cos\theta & \cos\varphi\cos\theta \end{bmatrix} \tag{11}$$

where $\boldsymbol{A}_s$ and $\boldsymbol{B}_s$ are the system matrix and control matrix at different equilibrium points, respectively; $\boldsymbol{x}$ is the state vector; and $\boldsymbol{u}$ is the control input vector.

The signal transmission and calculation process of the robot pilot can be considered as a constant time delay in the flight simulation. The servo process of the robot manipulators can be simplified as a first-order inertial element. The inertial parameter is an estimated value according to the dynamic performance of the servo motors. The helicopter-controlling mechanism contains mechanical transmission and is generally embedded with hydraulic servos. It transmits the deflection of the control sticks and pedals to the swashplate directions and attack angles of the rotor blades, resulting in inertia, pure time delay, and uncertainty disturbance during the flight. Since accurate mechanical transmission of the helicopter is difficult to achieve, the helicopter-controlling mechanism is approximated and introduced using second-order transfer functions in the flight simulations.

The flight simulation of the robot–helicopter system focused on the command tracking performance of the helicopter's longitudinal channel, lateral channel, yaw channel, and altitude channel. Each channel has an independent PID controller, and the PID parameters of the four controllers were initially tuned based on the flight simulation. The simulation results are illustrated in Fig. 16, showing that the helicopter can track the command signals of all the four channels. The dynamics of the helicopter's longitudinal channel and lateral channel are relatively complicated; the time delay and inertia introduced by the robot manipulators and the helicopter-controlling mechanism makes it more difficult to tune the PID parameters, resulting in increased overshot and tracking error in the simulation. The dynamics of the yaw channel and altitude channel are simple and highly linear. The time delay and inertia have little influence on the command tracking performance of these two channels, and the PID controllers realized a fast response speed and slight overshot.

Fig. 18. Ground station and visual display.

Ground obseration

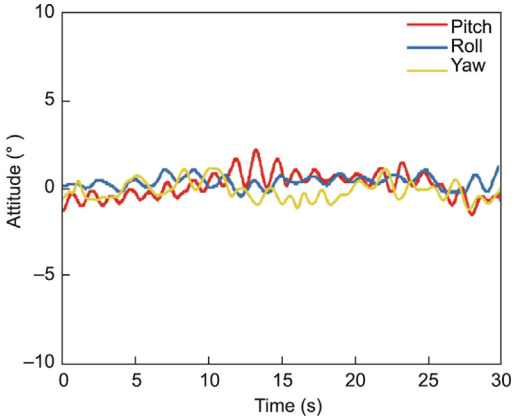

Fig. 19. Helicopter hovering.

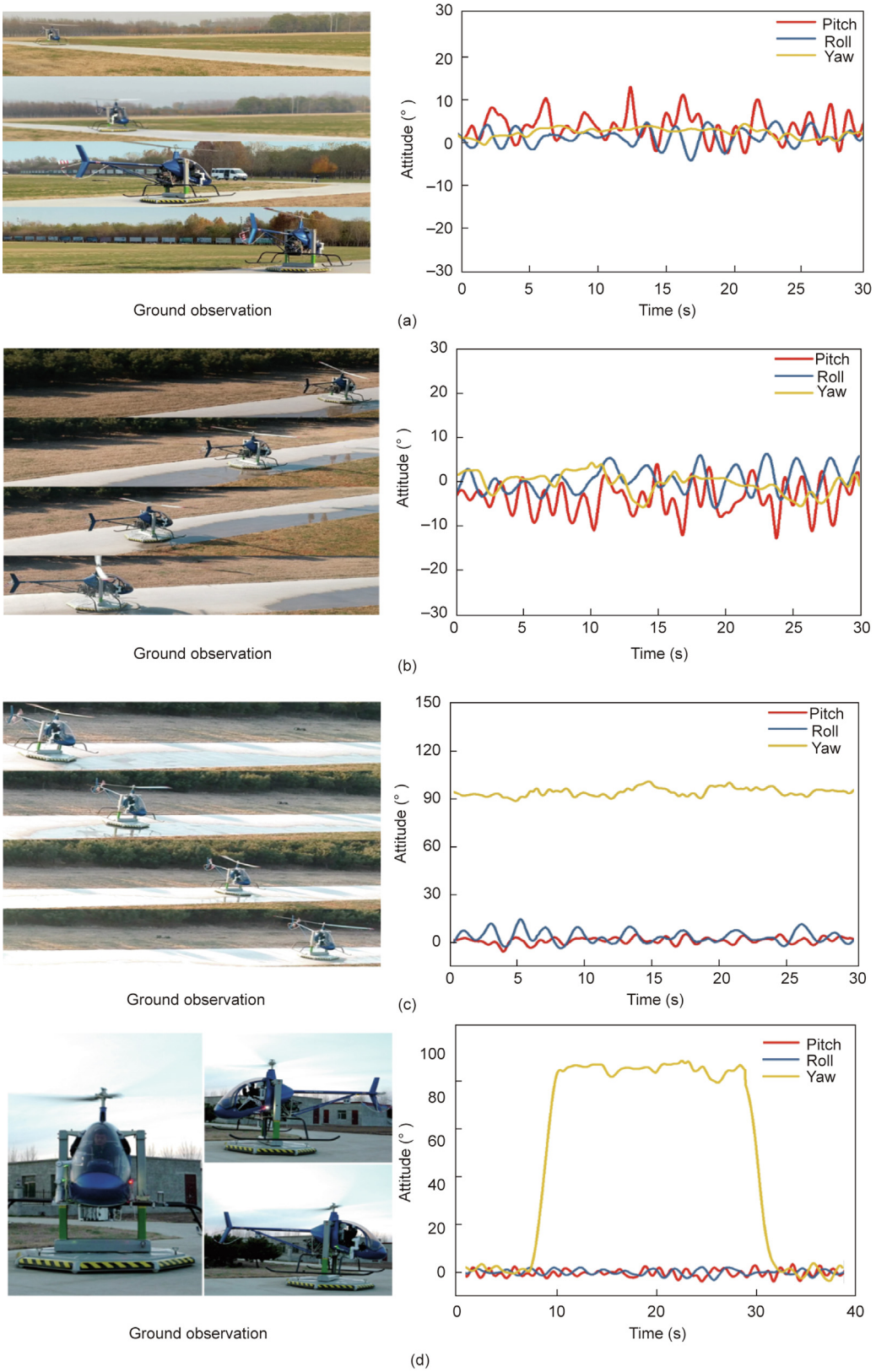

Fig. 20. Ground observation and flight attitude of different flight tasks realized by the robot pilot. (a) Forward flight; (b) backward flight; (c) side flight; (d) turning flight.

5. Experimental validation

5.1. Robot processing and ground station

A prototype of the robot pilot was processed and installed in the SVH-4 helicopter to carry out the ground test, as shown in Fig. 17. Since the cockpit space of the SVH-4 helicopter is small, the base of the 6-DOF manipulator is mounted at the landing skid of the helicopter, and the end-effector stretches over the cabin door to control the helicopter control stick. For most other helicopters and double-seater helicopters, the 6-DOF manipulator base can be installed in the cockpit or on the co-pilot seat. A robot torso structure was designed to assemble the mechanical leg, mechanical arm, and other equipment. We also adopted a hollow design for the robot torso in which to place the control box. The control box is made of aluminum alloy and has a manipulator controller and power supplies installed inside. On the left side of the control box is the test panel, which is used to configure the initial positions and drive settings of the robot manipulators. The flight controller and Global Positioning System (GPS) are installed at the left side of the helicopter landing skid to estimate the helicopter attitude and send control signals to the control box of the robot pilot.

The robot pilot is equipped with a head camera on the robot torso to monitor the scene outside the cockpit. The head camera is installed on a three-axis pan-tilt so that the camera can rotate along the three-axis directions and capture the scenes in all directions, like a human pilot. In addition, a camera box is installed at the tail beam of the helicopter to monitor the rear view, which further broadens the visual range of the robot pilot. Three cameras are mounted on the back and sides of the camera box, and a separate power supply is placed in the box.

A ground station was designed and built to assist in the piloting of the robot pilot, as shown in Fig. 18. The ground station has multiple screens, which can simultaneously display the flight state of the helicopter and the visual information sent back by the cameras. The ground station can also send control commands to the robot pilot through the joysticks installed on the platform. As a result, it enables human pilots to remotely control the robot pilot to fly the helicopter according to the screen displays of the ground station. Thus, the robot pilot realizes both automatic helicopter control and remote flight control, notably improving the adaptability and safety of the robot–helicopter system. For example, when the robot pilot does not work properly or the helicopter encounters emergency conditions, human pilots can retrieve control at the ground station and remotely control the robot to perform emergency operations through manual operation.

5.2. Flight test of the robot pilot

The robot manipulators were connected to the helicopter-controlling mechanisms to carry out the flight tests. The connections were examined in a ground test to ensure that the robot manipulators could quickly and accurately control the helicopter-controlling mechanisms and manipulate them to reach their limit positions. Then, the helicopter engine was activated and the robot pilot was set up to hover the helicopter. As illustrated in Section 4, we used four independent PID controllers to control the attitude of the helicopter. The PID parameters of the attitude controller were tuned after multiple hover tests; finally, the robot pilot was able to stably hover the helicopter, as shown in Fig. 19. A human pilot sat in the front seat of the cockpit to shut down the engine in case of emergency and did not participate in helicopter control. The attitude data of the helicopter hover process was recorded. The attitude oscillation was small, and the helicopter basically remained in a stable state under the control of the robot pilot.

Table 1
Attitude standard deviation during the flight tasks.

Flight task	Pitch (°)	Roll (°)	Yaw (°)
Hovering	0.70	0.33	0.53
Forward flight	3.06	1.87	1.08
Backward flight	3.42	2.78	2.31
Side flight	1.89	3.71	2.54
Turning flight	1.56	1.23	—

Since the robot pilot was able to effectively hover the helicopter, the flight tasks of a forward flight, backward flight, side flight, and turning flight were conducted. To fly, the SVH-4 helicopter must overcome the friction resistance between the supporting platform and the ground, which makes it easier for the helicopter to generate altitude turbulence and creates difficulties for the helicopter flight control. The flight tasks were realized by adding an outer speed control loop to the altitude controller of the robot pilot. The outer speed control loop uses proportional–differential (PD) controllers to force the helicopter to track a certain speed to realize the flight tasks. The parameters of both the inner attitude controllers and the outer speed controllers were further tuned during the flight tasks.

The test results of the flight tasks are shown in Fig. 20. Ideally, the helicopter should maintain a certain attitude during the flight tasks. Therefore, the standard deviation of the helicopter attitudes during the flight tests was calculated, as shown in Table 1, to evaluate the flight performance. In general, there are three main factors that may cause attitude oscillations: ① the time delay and control error of the robot servo process; ② discontinuous friction between the moving platform and the ground; and ③ the ground effect and damping caused by the whole supporting platform. Attitude oscillations during the helicopter's hovering flight were mainly caused by the ground effect and damping of the supporting platform. We studied the flight data of human pilots hovering the SVH-4 helicopter and found that attitude oscillation also occurred for such pilots and with an even greater magnitude, which indicates that the helicopter attitude is caused by the inherent characteristics of the SVH-4 helicopter. For the forward flight, backward flight, and side flight, the attitude oscillation is mainly caused by discontinuous ground friction. The attitude oscillation of the side flight is the most significant because of the strong lateral–directional coupling of the helicopter. Through the ground test, the robot manipulators showed a fast response speed and good control accuracy based on the direct-driving method. It can be speculated that, when the helicopter flies off the ground, it will demonstrate a significant improvement in flight performance and the robot pilot will be better able to control the helicopter. In summary, the test results indicate that the robot pilot is able to fly the helicopter and accomplish several flight tasks, verifying the effectiveness of the robot pilot presented in this research.

6. Conclusions

In this research, we first developed a helicopter robot pilot to serve as autonomous equipment that can independently fly a manned helicopter. The robot pilot provides a new way to reversibly convert manned helicopters into unmanned helicopters without executing complicated modifications on the original helicopter. The detailed design and implementation of the robot pilot were discussed. We adopted a modular method to design robot manipulators for each helicopter-controlling mechanism and integrated the manipulators using a torso structure. The control stick of the helicopter was operated by a 6-DOF manipulator, while the universal joint of the end-effector eliminated the motion constraint of the control stick. A mechanical arm and mechanical leg were proposed to control the collective and helicopter pedals, respectively. By

choosing an appropriate mechanism length, quasi-linear kinematic relations between the joint angles and helicopter control quantities were achieved. On this basis, we proposed a direct-driving method to let the PWM signals output by the helicopter flight controller directly drive the manipulator joints. From the perspective of the whole control flow of the robot–helicopter system, the direct-driving method unifies the helicopter flight controller and robot servo controller, effectively reducing the time delay and control error of the robot servo process and providing a convenient solution for the parameter tuning of the robot flight control.

A prototype of the presented robot pilot was processed and installed in an SVH-4 helicopter to conduct flight tests. A ground station was also developed to assist in piloting and realize functional requirements. Multiple tests were required to tune the PID parameters; finally, the robot pilot was able to fly the helicopter to accomplish flight tasks including helicopter hovering, forward flight, backward flight, side flight, and turning flight.

The robot pilot presented here can be further applied to other aircraft and is considered to have great potential for wide application. Future works should focus on improving the control performance of the robot pilot, as the test results show obvious attitude oscillations. Even though PID controllers are convenient to deploy and suitable for various system controls, their control capacity is still limited. Modern control methods or intelligent control methods could be used for the robot pilot in future.

Acknowledgments

This study was supported by the National Natural Science Foundation of China (11972059).

Compliance with ethics guidelines

Zibo Jin, Daochun Li, and Jinwu Xiang declare that they have no conflict of interest and financial conflicts to disclose.

References

[1] Mcfadyen A, Mejias L. A survey of autonomous vision-based see and avoid for unmanned aircraft systems. Prog Aerosp Sci 2016;80:1–17.
[2] Skowron M, Chmielowiec W, Glowacka K, Krupa M, Srebro A. Sense and avoid for small unmanned aircraft systems: research on methods and best practices. Proc Inst Mech Eng 2019;233(16):6044–62.
[3] Yang H, Lee Y, Jeon SY, Lee D. Multi-rotor drone tutorial: systems, mechanics, control and state estimation. Intell Serv Robot 2017;10(2):79–93.
[4] Lin Y, Gao F, Qin T, Gao W, Liu T, Wu W, et al. Autonomous aerial navigation using monocular visual–inertial fusion. J Field Rob 2018;35(1):23–51.
[5] Faessler M, Fontana F, Forster C, Mueggler E, Pizzoli M, Scaramuzza D. Autonomous, vision-based flight and live dense 3D mapping with a quadrotor micro aerial vehicle. J Field Robot 2016;33(4):431–50.
[6] Doukhi O, Lee DJ. Deep reinforcement learning for end-to-end local motion planning of autonomous aerial robots in unknown outdoor environments: real-time flight experiments. Sensors 2021;21(7):2534.
[7] Zhou Y, Lai S, Cheng H, Redhwan AHM, Wang P, Zhu J, et al. Toward autonomy of micro aerial vehicles in unknown and global positioning system denied environments. IEEE Trans Ind Electron 2021;68(8):7642–51.
[8] Shraim H, Awada A, Youness R. A survey on quadrotors: configurations, modeling and identification, control, collision avoidance, fault diagnosis and tolerant control. IEEE Aerosp Electron Syst Mag 2018;33(7):14–33.
[9] Kovalev IV, Voroshilova AA, Karaseva MV. On the problem of the manned aircraft modification to UAVs. J Phys Conf Ser 2019;1399(5):055100.
[10] Airforce Technology. QF-16 full scale aerial target. Report. New York City: Airforce-technology.com; 2016 Dec 8.
[11] Airforce Technology. Dominator MALE UAV. Report. New York City: Airforce-technology.com; 2011 Mar 7.
[12] Hardesty M, Guthrie D, Cerchie D. Unmanned little bird testing approach. In: Proceedings of the American Helicopter Society International—International Specialist Meeting on Unmanned Rotorcraft Systems 2009; 2009 Jan 20–22; Phoenix, AZ, USA. Fairfax: VFS; 2009. p. 496–507.
[13] Graham J, Tadghighi H, Caldwell D, Cerchie D. Unmanned little bird analytic tools. In: Proceedings of the American Helicopter Society International—International Specialists Meeting on Unmanned Rotorcraft 2009; 2009 Jan 20–22; Phoenix, AZ, USA. Fairfax: VFS; 2009. p. 518–28.
[14] Graham J, Caldwell D, Dockter G, Cerchie D. Unmanned Little Bird command and control. In: Proceedings of the American Helicopter Society International—International Specialists Meeting on Unmanned Rotorcraft 2009; 2009 Jan 20–22; Phoenix, AZ, USA. Fairfax: VFS; 2009. p. 335–8.
[15] Jeong H, Kim J, Shim DH. Development of an optionally piloted vehicle using a humanoid robot. In: Proceedings of the 52nd AIAA Aerospace Sciences Meeting—AIAA Science and Technology Forum and Exposition; 2014 Jan 13–17; National Harbor, MD, USA. Reston: AIAA; 2014. p. 1165.
[16] Kreitmair-Steck W, Haisch S, Hess S, Jank, S. Eurocopter research on pilot assistance for rotorcraft. In: Proceedings of Enhanced and Synthetic Vision 2009. SPIE Defense, Security, and Sensing 2009; 2009 Apr 13–17; Orlando, FL, USA. Bellingham: SPIE; 2009. p. 78–87.
[17] Greiser S, Lantzsch R, Wolfram J, Wartmann J, Müllhäuser M, Lüken T, et al. Results of the pilot assistance system "assisted low-level flight and landing on unprepared landing sites" obtained with the ACT/FHS research rotorcraft. Aerosp Sci Technol 2015;45:215–27.
[18] Gierszewski D, Nagarajan P, Jaisle J, Krammer C, Maly M, Holzapfel F. Demonstration of a procedure-based approach to functional analysis for an optionally piloted vehicle. In: Proceedings of the AIAA Scitech Forum; 2021 Jan 11–15 & 19–21; online Reston: AIAA; 2021. p. 1635.
[19] Wu W, Zhang Y, Liu J, Zhou S, Mei D. Overall architecture design of new generation intelligent cockpit. Hangkong Xuebao 2016;37(1):290–9. Chinese.
[20] Lounis C, Peysakhovich V, Causse M. Intelligent cockpit: eye tracking integration to enhance the pilot-aircraft interaction. In: Proceedings of the 2018 Symposium on Eye Tracking Research and Applications; 2018 Jun 14–17; Warsaw, Poland. New York City: ACM; 2018. p. 74.
[21] Liang B, Chen Y, Wu H. A conception of flight test mode for future intelligent cockpit. In: Proceedings of the 2020 Chinese Automation Congress (CAC); 2020 Nov 6–8; Shanghai, China. IEEE; 2020. p. 3260–4.
[22] Liu J, Gardi A, Ramasamy S, Lim Y, Sabatini R. Cognitive pilot–aircraft interface for single-pilot operations. Knowl Base Syst 2016;112:37–53.
[23] Vu KPL, Lachter J, Battiste V, Strybel TZ. Single pilot operations in domestic commercial aviation. Hum Factors 2018;60(6):755–62.
[24] Ernest N, Cohen K, Kivelevitch E, Schumacher C, Casbeer D. Genetic fuzzy trees and their application towards autonomous training and control of a squadron of unmanned combat aerial vehicles. Unmanned Syst 2015;3(3):185–204.
[25] Zheng N, Liu Z, Ren P, Ma Y, Chen S, Yu S, et al. Hybrid-augmented intelligence: collaboration and cognition. Front Inf Technol Electron Eng 2017;18(2):153–79.
[26] Young SH. Aircrew Labor In-Cockpit Automation System (ALIAS). Report. Arlington: DARPA.
[27] Kucinski W. Phase three of DARPA's ALIAS aircraft automation system continues. Report. Warrendale: SAE International; 2018 Oct 30.
[28] Johnson M, Beane M, Mindell D, Ryan J. Knowledge management for rapidly extensible collaborative robots. In: Proceedings of the HCII 2019: Human Interface and the Management of Information. Visual Information and Knowledge Management; 2019 Jul 26–31; Orlando, FL, USA. Cham: Springer; 2019. p. 503–23.
[29] OUTREACH@DARPA.MIL. ALIAS equipped Black Hawk helicopter completes first uninhabited flight. Report. Arlington: DARPA; 2022 Feb 8.
[30] Song H, Shin H, You H, Hong J, Shim DH. Toward autonomous aircraft piloting by a humanoid robot: hardware and control algorithm design. In: Proceedings of the 2016 IEEE/RSJ International Conference on Intelligent Robots and Systems (IROS); 2016 Oct 9–14; Daejeon, Republic of Korea. IEEE; 2016. p. 398–403.
[31] Jeong H, Shim DH, Cho S. A Robot-Machine Interface for full-functionality automation using a humanoid. In: Proceedings of the 2014 IEEE/RSJ International Conference on Intelligent Robots and Systems; 2014 Sep 14–18; Chicago, IL, USA. IEEE; 2014. p. 4044–9.
[32] Airforce technology. US AFRL conducts debut flight of ROBOpilot unmanned air system. Report. New York City: Airforce-technology.com; 2019 Aug 16.
[33] Air Force Research Laboratory Public Affairs. ROBOpilot Unmanned Air Platform returns to flight. Report. Wright-Patterson Air Force Base: AFRL; 2020 Sep 28.
[34] Jin Z, Li D, Wang Z. Research on the operating mechanicals of the helicopter robot pilot. IOP Conf Series Mater Sci Eng 2020;887(1):012022.
[35] Ruderman M, Hoffmann F, Bertram T. A Matlab-based framework for the remote control of a 6-DOF robotic arm for education and research in control theory. IFAC Proc 2012;45(11):366–71.
[36] Gao M, Chen D, Yang Y, He Z. A fixed-distance planning algorithm for 6-DOF manipulators. Ind Rob Int J 2015;42(6):586–99.
[37] Kucuk S, Bingul Z. The inverse kinematics solutions of industrial robot manipulators. In: Proceedings of the IEEE International Conference on Mechatronics; 2004 Jun 5; Istanbul, Turkey. IEEE; 2004. p. 274–9.
[38] Kucuk S, Bingul Z. Inverse kinematics solutions for industrial robot manipulators with offset wrists. Appl Math Model 2014;38(7–8):1983–99.
[39] Heffley RK, Jewell WF, Lehman JM, Van Winkle RA. A compilation and analysis of helicopter handling qualities data. Report. Moffett Field: NASA Ames Research Center; 1979 Aug. Report No.: NASA CR-3144. Contract No.: NAS2-9344.